Received 18 March 2022; revised 6 May 2022 and 31 May 2022; accepted 18 June 2022. Date of publication 22 June 2022; date of current version 11 July 2022.
The review of this article was arranged by Editor K. Cheng.

Digital Object Identifier 10.1109/JEDS.2022.3185324

Real-Time Switching Dynamics in STT-MRAM

N. YAZIGY[1], J. POSTEL-PELLERIN[1], V. DELLA MARCA[1], K. TERZIYAN[1], R. C. SOUSA[2], P. CANET[1], AND G. DI PENDINA[2]

1 Aix-Marseille University, CNRS, IM2NP, 13451 Marseille, France
2 University Grenoble Alpes, CNRS, CEA-SPINTEC, CEA, 38000 Grenoble, France

CORRESPONDING AUTHOR: N. YAZIGY (e-mail: nicole.yazigy@im2np.fr)

This work was supported by the the French National Research Agency (ANR) under Grant ANR-19-CE39-0010.

ABSTRACT In this paper a new experimental technique for measuring the switching dynamics and extracting the energy consumption of Spin Transfer Torque MRAM (STT-MRAM) device is presented. This technique is performed by a real-time current reading while a pulsed bias is applied. The switching from a high resistive state, anti-parallel (AP) alignment, to a low resistive state, parallel (P) alignment, is investigated as well as the impact of the cell diameter on the switching parameters. We demonstrate that preswitching and switching times and energies have a log-linear relationship with the applied voltage. Increasing the applied voltage leads to a higher spin torque on the free layer in a shorter time. This decreases the time needed to change the magnetization orientation of this layer, thus the time required before the switching occurs. We have also shown that for a given applied voltage, the smaller the cell the longer the time before switching. For low applied voltages, the preswitching time increases exponentially dominating the whole reversal time. The longer switching times can be explained by a lower Joule heating not sufficient to induce the thermally activated reversal process. This phenomenon is accentuated for smaller cells, where the heating is more significant and the time before switching is shorter than for larger cells.

INDEX TERMS Magnetic switching, MRAM devices, perpendicular magnetic tunnel junction, spin transfer torque.

I. INTRODUCTION

MAGNETIC Random Access Memory (MRAM) has been developed in several generations so far, in particular STT-MRAM which is one of the most attractive emerging memories candidates [1], [2]. For high-density STT-MRAM integration, perpendicular magnetic tunnel junctions (p-MTJs) are more energy efficient due to stronger perpendicular anisotropy and reduced energy levels needed to perform switching are expected to achieve lower critical current density and greater thermal stability, thus lower bias voltage. A CoFeB/MgO/CoFeB based tunnel junction represents the core component of this p-MTJ stack, where spin transport phenomena such as tunneling magnetoresistance and magnetization reversal of the storage layer by STT occur [3]–[5]. Fig. 1.a shows a High-Resolution Transmission Electron Microscopy (HRTEM) of the whole stack used in our study. The resistance of an MTJ device depends on the relative orientation of the magnetization of the free and fixed ferromagnetic (FM) layers (Fig. 1.b and Fig. 1.c) due to spin-dependent tunneling and is quantified by tunnel magnetoresistance ratio (TMR). The free FM's magnetization direction can be changed either by applying a static magnetic field higher than the coercivity of the FM layer or by forcing a spin-polarized current through the device. The transverse component of spin current gets absorbed in the FM, implying a torque on the magnetization of the FM known as the Spin Transfer Torque (STT) effect [6]–[8]. Fig. 1.b and Fig. 1.c also show the two possible states: the high-resistive AP state and the low-resistive P state that usually represent "1" and "0" logical states respectively.

The time required for this change of state of the STT-MRAM cell and its dependence on the voltage used during programming are key criteria. Recent studies have simulated this behavior but very few real-time measurements studies exist to confirm the proposed reversal mechanisms [6], [9], [10].

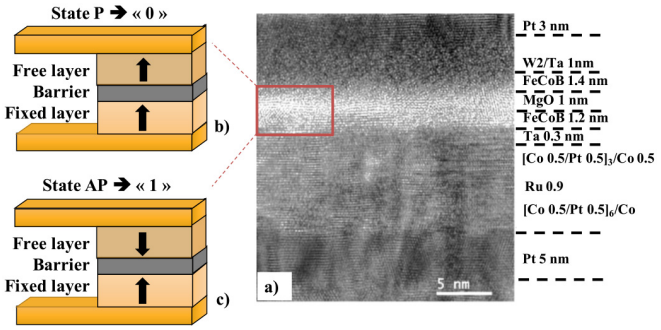

FIGURE 1. **(a) HRTEM images of p-MTJ of STT-MRAM stack [3], (b) P state and (c) AP state configurations.**

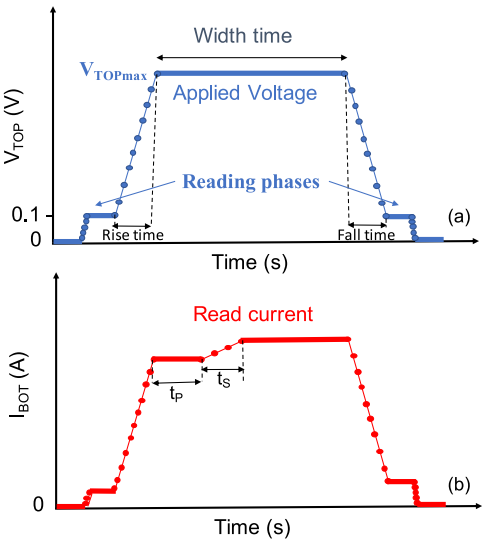

FIGURE 2. **(a) Applied bias voltage pattern showing the rise, width and fall times and the reading phase at 0.1 V, (b) read current and the extraction of the preswitching (t_P) and the switching (t_S) times.**

This article proposes an experimental evaluation of the switching dynamics thereby we chose one of the two STT-MRAM transitions which is the passage from AP to the P state of the STT-MRAM cell. Using a simple method where a pulsed bias voltage is applied while reading the current at the same time will allow the extraction of the real-time dynamics of the switching phenomenon. The novelty of our work lies in the distinction between two phases called "preswitching" and "switching" while in previous works these two phases were combined in a single global phase called "switching" [11]. The separation is important because in reality two successive phases occur as demonstrated in [11]–[14]. In the first phase, the nucleation of the domain wall, during what we call in this paper the "Preswitching time", spins are accumulated in the free layer and the nucleation takes place. Then, during the second phase, the propagation phase of the domain wall of the entire device, called "Switching" in this paper, all the spins reverse. We want to study the behavior of each of these mechanisms with applied voltage and diameter.

Fig. 2.a. presents the shape of the pulse which consists of an initial reading phase at 0.1V to confirm the AP state

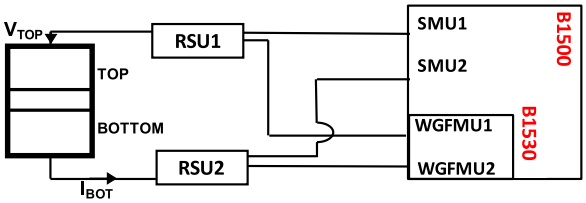

FIGURE 3. **Measurement setup a prober and an Analyzer B1500 of Keysight Technologies brand.**

TABLE 1. **Main characteristics of the three considered samples.**

Diameter (nm)	TMR %	RA (Ω. m^2)
80	35.4	43.73
100	32.5	34.55
150	29.7	53.00

followed by a rise time. This is followed by a pulse up to the maximum voltage value (VTOPmax). This phase has the role of measuring and detecting the dynamic current transition. A second reading phase at 0.1V, following a fall time, enables the extraction of the resistance value after switching. The time between the start of the pulse rise time and the beginning of the current induced switching is called preswitching time (t_P). On the other hand, the switching time (t_S) is defined as the time required for the cell to pass from a low-current level to a high-current level, as described in Fig. 2.b.

II. EXPERIMENTAL SETUP

Our samples are integrated in a 100mm wafers we fabricated in an academic cleanroom within the CEA facilities. They are characterized using a Keysight B1500A semiconductor device analyzer to apply signals for Quasi-Static Measurements (QSM) through Source Monitor Units (SMU) while Pulsed Measurements (PM) are carried out by Waveform Generator Fast Measurement Units (WGFMU in a B1530 module), as shown in Fig. 3. and explained in a previous work [15]. The Remote-sense and Switch Unit (RSU) modules enable the link with the probes and the device under test [16]. The Bottom Electrode (BE) current (IBOT) is measured instead of the Top Electrode (TE) current (ITOP) to avoid drift current due to the capacitance of the connecting wires. We applied the bias voltage (VTOP) on the TE of the MTJ while the BE is grounded.

In order to study the size effect on the switching phenomenon, we investigated three different cells with their respective diameters, TMR and Resistance-Area (RA) products shown in Table 1.

A. QUASISTATIC MEASUREMENT (QSM)

Fig. 4. presents the quasi-static current-voltage characteristics where the voltage applied VTOP is swept from zero to a positive switching bias and then swept to a negative switching bias, measuring the IBOT current, for cells with different diameters. The switching voltages are affected by the sweep ramp speed that cannot be exactly controlled in

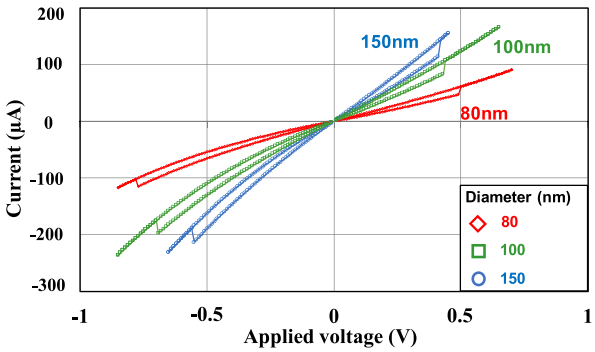

FIGURE 4. Quasi-static measured current (IBOT) as a function of the applied voltage (VTOP) for cells with diameters 80 nm, 100 nm and 150 nm.

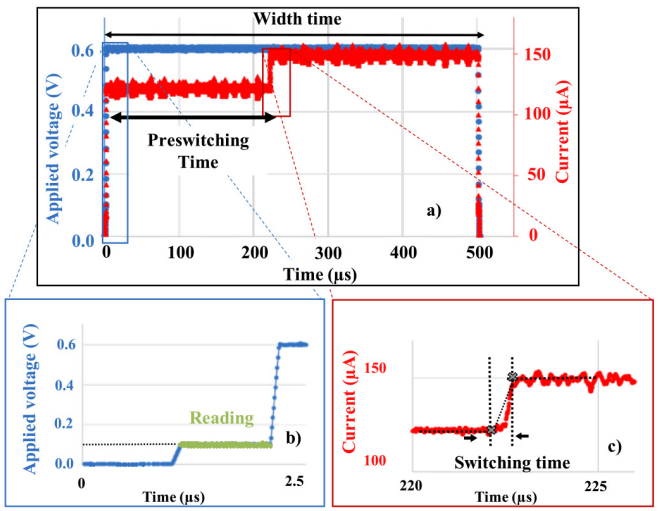

FIGURE 5. (a) Experimental result showing applied voltage and measured current for VTOPmax = 0.6V, width time = 500μs, sampling time = 10 ns and the rise-fall time = 100 ns, as well as definition of preswitching time. (b) reading voltage and (c) switching time.

QSM. This limitation implies to develop a dynamic measurement mode based on pulsed measurements (PM). This quasi-static study provides a benchmark for further work based on pulsed measurements from which we could extract preswitching and switching time. The reading of the AP or P state of the cell is performed using a 0.1V QSM.

B. PULSED MEASUREMENTS (PM)

In this paper we focus on the switching from AP to P state. The method consists in applying the pattern, described in Fig. 2.a., on the top electrode after ensuring that the cell is initially in AP state. The total number of measurement points is limited by the measurement setup to 10^5 sampling points of which in all our measurements we applied the rise-fall time equals to 10 sampling points (which is short enough not to impact the measurement and fast enough not to have an overshoot). Note that sampling of PM method limits the precision of switching time measurement.

The switching from high to a low resistive state can be observed Fig. 5. We can notice that the switch takes place gradually because the initial nucleation of a magnetic domain

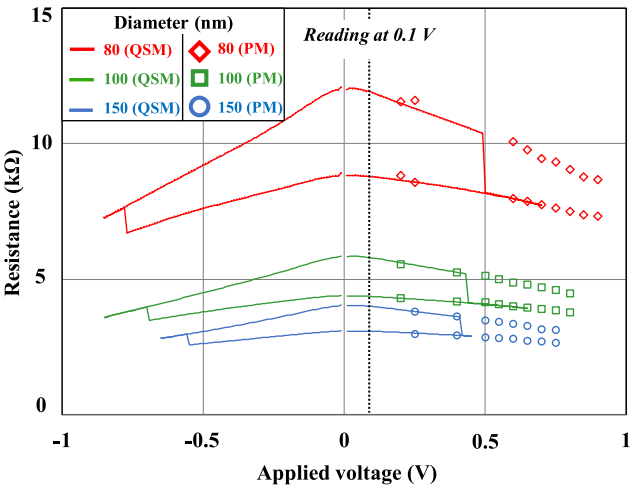

FIGURE 6. Resistance as a function of the applied voltage in quasi-static mode (Fig. 4), as well as their corresponding average pulse mode resistances over 30 measurements.

is followed by a phase of propagation of the wall through the rest of the free layer [11]–[14]. Note that with the arbitrary pulse generators we are able to modify the pulse duration (width time), VTOPmax as well as the rise and fall times.

The experimental results are presented in the next section.

III. RESULTS

In order to compare quasi-static and pulse switching results we show in Fig. 6 values of the calculated resistance values from Fig. 4. The extraction of low resistance state values in QSM is possible for every positive voltage before the cell breakdown while it is impossible for the high resistance state, because of the switching occurrence. Moreover, we carried out a set of dynamic characterizations demonstrating that the AP to P transition in pulsed mode leads to higher switching voltages because of the shorter pulse width compared to the QSM (symbols in Fig. 6.).

For lower applied voltages, the pulse width time is long enough and thus comparable for the two experimental methods. The dynamic characterizations have been repeated thirty times for each VTOPmax to limit the cycle-to-cycle variability. The preswitching time (t_P) and the switching time (t_S) have been extracted and their mean values are plotted in Fig. 7 and Fig. 8 respectively. We can notice that the results obtained for 100 and 150 nm are quite close. The similar switching behaviors can be explained by the fact that the Parallel resistance R_P value is neither proportional to the diameter nor to the device area as shown in Fig. 6. as well as in [11]. The switching behavior is led by the R_P value, rather than the diameter or area.

IV. DISCUSSION

The preswitching and switching times showed a stochastic behavior. The preswitching time is reduced when increasing the applied bias due to a larger spin current passing through the magnetic tunnel junction device. For a 100 nm diameter

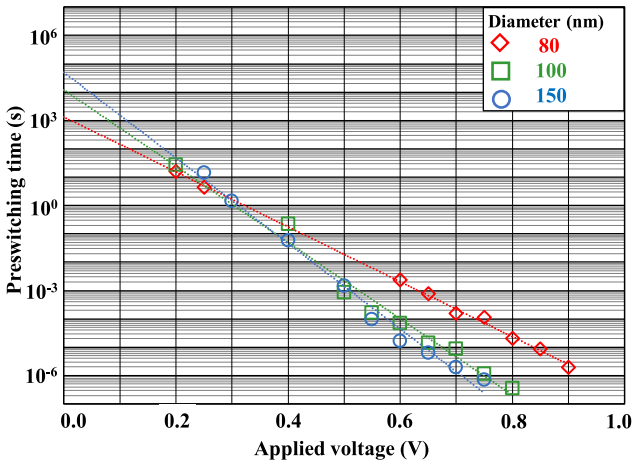

FIGURE 7. The average over 30 measurements of the preswitching time for each of the 3 cells of diameter 80, 100 and 150 nm.

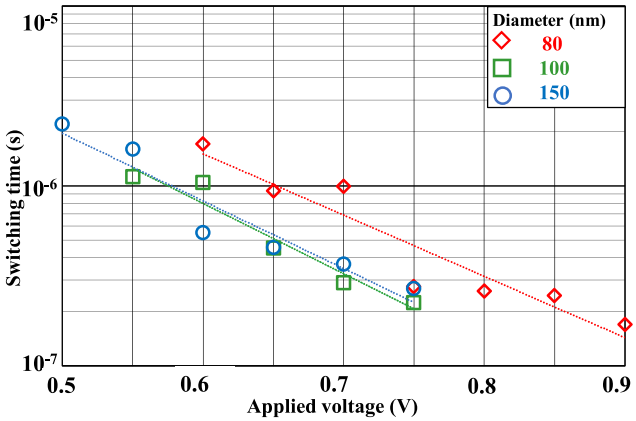

FIGURE 8. The average over 30 measurements of the switching time for each of the 3 cells of diameter 80, 100 and 150 nm.

cell the preswitching time decreases by a ratio of 10^8 when the applied voltage increases from 0.2 to 0.8V, while the switching time slightly decreases with the applied voltage increases. The preswitching and the switching times decrease with the current increase which corresponds to the result obtained in [17] where the mean value of the switching time of the MTJ decreased with the current increase.

On the other hand, for the same applied voltage the preswitching time decreases when the diameter increases, which can be explained by lower retention in larger diameter sizes [18]–[20], likely because the probability of defects and reversal nucleation sites increases for larger diameters.

The observed exponential dependence, for t_P and t_S with the pulse voltage, is expressed in (1) and (2).

$$t_P = t_{0P}.e^{-V_{TOP}/V_{0P}} \quad (1)$$

$$t_S = t_{0S}.e^{-V_{TOP}/V_{0S}} \quad (2)$$

Where "P" stands for preswitching and "S" stands for switching.

The model parameters t_{0P}, t_{0S}, V_{0P} and V_{0S} are shown in Table 2.

TABLE 2. Values of the model parameters in equations (1) and (2).

Diameter (nm)	t_{0P} (ks)	V_{0P} (mV)	t_{0S} (µs)	V_{0S} (mV)
80	1	45	200	128
100	10	32	200	111
150	50	29	100	116

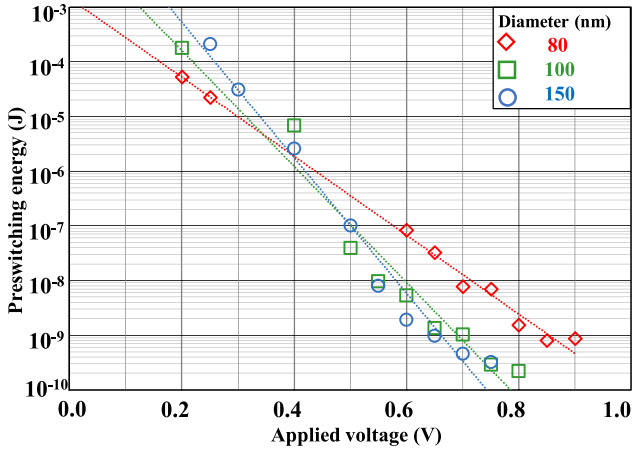

FIGURE 9. Average over 30 measurements of the preswitching energy for each of the three cell diameters 80, 100 and 150 nm.

TABLE 3. Values of the model parameters in equation (3) and (4).

Diameter (nm)	E_{0P} (mJ)	V_{0P} (mV)	E_{0S} (nJ)	V_{0S} (V)
80	1.4	60	0.59	0,26
100	21	40	1.71	0,18
150	158	30	2.34	0,19

Finally, in this section, we use the dynamic results to represent the electrical energy of the MTJ based STT-MRAM. The preswitching energy is plotted in Fig. 9.

The energy is the integral of the electric power over time. The model of preswitching and switching energies (E_P) and (Es) are expressed in (3) and (4).

$$E_P = E_{0P}.e^{-V_{TOP}/V_{0P}} \quad (3)$$

$$E_S = E_{0S}.e^{-V_{TOP}/V_{0S}} \quad (4)$$

The model parameters E_{0P}, E_{0S}, V_{0P} and V_{0P} are shown in Table 3.

The preswitching energy that corresponds to the energy dissipated before AP to P transition occurs is significantly reduced when the cell diameter is increased [21]. This result is consistent with the increase of the resistance when the cell's size decreases for biases higher than 0.3V. The current flow in the MTJ is thus decreased and a longer preswitching time is required to switch to the parallel state. For an applied voltage lower than 0.3V, the dissipated preswitching energy rises for larger diameters, which is caused by thermal dissipation in the cell as a result of the long pulse width times [22]. This observation is consistent with the assumption of a thermally activated reversal mechanism. In the Fig. 10. the switching energy also shows a downward log-linear behavior. We remind that this paper aims at presenting a new methodology for the extraction of preswitching

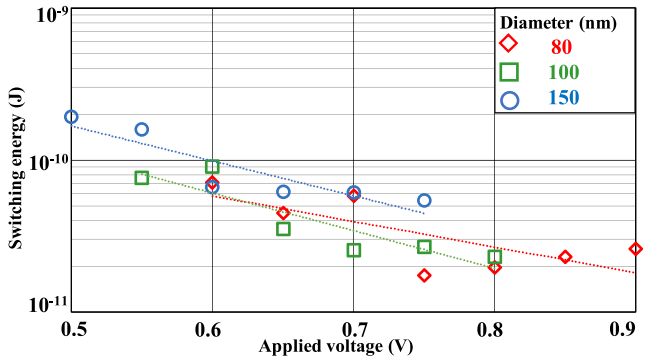

FIGURE 10. Average over 30 measurements of the switching energy for each of the three cell diameters 80, 100 and 150 nm.

and switching times in the AP to P state transition but it is fully applicable to the P to AP state transition since times involved in both transitions are comparable and reachable with our equipment despite the switching voltage asymmetry. In another study we propose the investigation of both transitions, also considering the impact of temperature [23].

V. CONCLUSION

In this paper we propose an experimental technique to measure the real-time reversal of AP to P state switching time in STT-MRAM cells. The time required to program the MTJ is greater when the diameter of the latter enlarges. The reversal can be decomposed in a preswitching time leading to the cell commutation and the switching time itself. We have also investigated the impact of the magnitude of the applied voltage on the t_P, as well as the t_S that is almost constant of the order of a few hundred of nanoseconds for the three different cell sizes. The switching energy has a log-linear relationship with the applied voltage. The cell switching event can be divided into two regimes, the thermally activated regime and the processional switching regime. For long write pulses and low applied voltage, the switching is dominated by thermal activation. As a result, the switching time was less than or equal to the sampling time. For short pulses, at high applied voltages, the switching is governed by the conservation of the spin angular momentum of the electrons. In this regime, the switching energy is inversely proportional to the pulse width and increases sharply with decreasing pulse widths. Finally, this innovative experimental study enabled to correlate fabricated device behavior with state-of-the-art theoretical results.

REFERENCES

[1] M. Kharbouche-Harrari *et al.*, "MRAM: From STT to SOT, for security and memory," in *Proc. Conf. Des. Circuits Integr. Syst. (DCIS)*, 2018, pp. 1–6, doi: 10.1109/dcis.2018.8681468.

[2] M. H. Kryder and S. K. Chang, "After hard drives—What comes next?" *IEEE Trans. Magn.*, vol. 45, no. 10, pp. 3406–3413, Oct. 2009, doi: 10.1109/tmag.2009.2024163.

[3] J. Chatterjee, E. Gautier, M. Veillerot, R. C. Sousa, S. Auffret, and B. Dieny, "Physicochemical origin of improvement of magnetic and transport properties of STT-MRAM cells using tungsten on FeCoB storage layer," *Appl. Phys. Lett.*, vol. 114, no. 9, 2019, Art. no. 92407, doi: 10.1063/1.5081912.

[4] Y.-J. Chang, A. Canizo-Cabrera, V. Garcia-Vazquez, Y.-H. Chang, and T.-H. Wu, "Perpendicular magnetic tunnel junctions with synthetic antiferromagnetic pinned layers based on [Co/Pd] multilayers," *J. Appl. Phys.*, vol. 113, no. 17, 2013, Art. no. 17B909, doi: 10.1063/1.4799974.

[5] D. Apalkov, B. Dieny, and J. M. Slaughter, "Magnetoresistive random access memory," *Proc. IEEE*, vol. 104, no. 10, pp. 1796–1830, Oct. 2016, doi: 10.1109/JPROC.2016.2590142.

[6] A. Sharma, A. A. Tulapurkar, and B. Muralidharan, "Proposal for energy efficient spin transfer torque-magnetoresistive random access memory device," *J. Appl. Phys.*, vol. 129, no. 23, Jun. 2021, Art. no. 233901, doi: 10.1063/5.0052693.

[7] A. Brataas, A. D. Kent, and H. Ohno, "Current-induced torques in magnetic materials," *Nat. Mater.*, vol. 11, no. 5, pp. 372–381, 2012, doi: 10.1038/nmat3311.

[8] W. H. Butler, X. G. Zhang, T. C. Schulthess, and J. M. MacLaren, "Spin-dependent tunneling conductance of Fe | MgO | Fe sandwiches," *Phys. Rev. B, Condens. Matter Mater. Phys.*, vol. 63, no. 5, 2001, Art. no. 54416, doi: 10.1103/physrevb.63.054416.

[9] G. Hu *et al.*, "Reliable five-nanosecond writing of spin-transfer torque magnetic random-access memory," *IEEE Magn. Lett.*, vol. 10, 2019, Art. no. 4504304, doi: 10.1109/LMAG.2019.2928243.

[10] S. Shi, Y. Ou, S. V. Aradhya, D. C. Ralph, and R. A. Buhrman, "Fast low-current spin-orbit-torque switching of magnetic tunnel junctions through atomic modifications of the free-layer interfaces," *Phys. Rev. Appl.*, vol. 9, no. 1, Jan. 2018, Art. no. 11002, doi: 10.1103/PhysRevApplied.9.011002.

[11] T. Devolder, A. Le Goff, and V. Nikitin, "Size dependence of nanosecond-scale spin-torque switching in perpendicularly magnetized tunnel junctions," *Phys. Rev. B, Condens. Matter*, vol. 93, no. 22, 2016, Art. no. 224432, doi: 10.1103/physrevb.93.224432.

[12] J. Guenole *et al.*, "Achieving sub-ns switching of STT-MRAM for future embedded LLC applications through improvement of nucleation and propagation switching mechanisms," in *Proc. IEEE Symp. VLSI Technol.*, 2016, pp. 1–2, doi: 10.1109/VLSIT.2016.7573362.

[13] P. Bouquin, S. Rao, G. S. Kar, and T. Devolder, "Size dependence of spin-torque switching in perpendicular magnetic tunnel junctions," *Appl. Phys. Lett.*, vol. 113, Nov. 2018, Art. no. 222408.

[14] J. G. Alzate *et al.*, "2 MB array-level demonstration of STT-MRAM process and performance towards L4 cache applications," in *Proc. IEEE Int. Electron Devices Meeting (IEDM)*, 2019, pp. 1–4, doi: 10.1109/IEDM19573.2019.8993474.

[15] V. D. Marca, J. Postel-Pellerin, T. Kempf, A. Regnier, P. Chiquet, and M. Bocquet, "Quantitative correlation between flash and equivalent transistor for endurance electrical parameters extraction," *Microelectron. Rel.*, vols. 88–90, pp. 159–163, Sep. 2018, doi: 10.1016/j.microrel.2018.06.116.

[16] H. Aoyama. "B1500A Semiconductor Device Analyzer." [Online]. Available: www.keysight.com

[17] R. de Rose, G. Carangelo, M. Lanuzza, F. Crupi, G. Finocchio, and M. Carpentieri, "Impact of voltage scaling on STT-MRAMs through a variability-aware simulation framework," in *Proc. 14th Int. Conf. Synth. Model. Anal. Simul. Methods Appl. Circuit Des. (SMACD)*, Jul. 2017, pp. 1–4, doi: 10.1109/SMACD.2017.7981583.

[18] T. Kishi *et al.*, "Lower-current and fast switching of a perpendicular TMR for high speed and high density spin-transfer-torque MRAM," in *Proc. IEEE Int. Electron Devices Meeting*, 2008, pp. 1–4, doi: 10.1109/IEDM.2008.4796680.

[19] T. Devolder *et al.*, "Material developments and domain wall-based nanosecond-scale switching process in perpendicularly magnetized STT-MRAM cells," *IEEE Trans. Magn.*, vol. 54, no. 2, pp. 1–9, Feb. 2018, doi: 10.1109/TMAG.2017.2739187.

[20] T. S. Santos *et al.*, "Ultrathin perpendicular free layers for lowering the switching current in STT-MRAM," *J. Appl. Phys.*, vol. 128, no. 11, Sep. 2020, Art. no. 113904, doi: 10.1063/5.0022576.

[21] Y. Lu *et al.*, "Fully functional perpendicular STT-MRAM macro embedded in 40 nm logic for energy-efficient IOT applications," in *Proc. IEEE Int. Electron Devices Meeting (IEDM)*, 2015, pp. 1–4, doi: 10.1109/IEDM.2015.7409770.

[22] K. Munira, W. H. Butler, and A. W. Ghosh, "A quasi-analytical model for energy-delay-reliability tradeoff studies during write operations in a perpendicular STT-RAM cell," *IEEE Trans. Electron Devices*, vol. 59, no. 8, pp. 2221–2226, Aug. 2012, doi: 10.1109/TED.2012.2198825.

[23] N. Yazigy *et al.*, "Experimental analysis on stochastic behavior of preswitching time in STT-MRAM," in *Proc. ESREF*, 2022.